International Journal of Coal Geology 98 (2012) 110–127

Contents lists available at SciVerse ScienceDirect

International Journal of Coal Geology

journal homepage: www.elsevier.com/locate/ijcoalgeo

Analyses of geological and hydrodynamic controls on methane emissions experienced in a Lower Kittanning coal mine

C. Özgen Karacan *, Gerrit V.R. Goodman

NIOSH, Office of Mine Safety and Health Research, Pittsburgh, PA 15236, United States

ARTICLE INFO

Article history:
Received 14 February 2012
Received in revised form 1 April 2012
Accepted 2 April 2012
Available online 28 April 2012

Keywords:
Coal mining
Methane control
Lower Kittanning coal
Geostatistics
Sequential Gaussian simulation

ABSTRACT

This paper presents a study assessing potential factors and migration paths of methane emissions experienced in a room-and-pillar mine in Lower Kittanning coal, Indiana County, Pennsylvania. Methane emissions were not excessive at idle mining areas, but significant methane was measured during coal mining and loading. Although methane concentrations in the mine did not exceed 1% limit during operation due to the presence of adequate dilution airflow, the source of methane and its migration into the mine was still a concern. In the course of this study, structural and depositional properties of the area were evaluated to assess complexity and sealing capacity of roof rocks. Composition, gas content, and permeability of Lower Kittanning coal, results of flotation tests, and geochemistry of groundwater obtained from observation boreholes were studied to understand the properties of coal and potential effects of old abandoned mines within the same area. These data were combined with the data obtained from exploration boreholes, such as depths, elevations, thicknesses, ash content, and heat value of coal. Univariate statistical and principal component analyses (PCA), as well as geostatistical simulations and co-simulations, were performed on various spatial attributes to reveal interrelationships and to establish area-wide distributions.

These studies helped in analyzing groundwater quality and determining gas-in-place (GIP) of the Lower Kittanning seam. Furthermore, groundwater level and head on the Lower Kittanning coal were modeled and flow gradients within the study area were examined. Modeling results were interpreted with the structural geology of the Allegheny Group of formations above the Lower Kittanning coal to understand the potential source of gas and its migration paths. Analyses suggested that the source of methane was likely the overlying seams such as the Middle and Upper Kittanning coals and Freeport seams of the Allegheny Group. Simulated groundwater water elevations, gradients of groundwater flow, and the presence of recharge and discharge locations at very close proximity to the mine indicated that methane likely was carried with groundwater towards the mine entries. Existing fractures within the overlying strata and their orientation due to the geologic conditions of the area, and activation of slickensides between shale and sandstones due to differential compaction during mining, were interpreted as the potential flow paths.

Published by Elsevier B.V.

1. Introduction

The presence of methane gas in the coal mine environment represents one of the greatest dangers to the underground work force. In concentrations of 5 to 15% by volume in air, a methane–air mixture can explode violently in the presence of a spark or other ignition source, leading to injuries or significant loss of life. Methane explosions at the Jim Walter Resources No. 5 mine in 2001, the Consol Energy McElroy mine in 2003, and the International Coal Group Sago mine and the Kentucky Darby LLC Darby No. 1 mine in 2006 resulted in 33 fatalities and 8 injuries. Most recently, an explosion at the Massey Energy Upper Big Branch mine in 2010 resulted in 29 fatalities and 2 injuries. The dangers of methane accumulations in the underground mine environment cannot be ignored.

Dangerous accumulations of methane gas are causes for concern at any location in an underground mine environment. However, prevention of excessive methane levels is most critical where coal is mined and loaded; as multiple ignition sources can be present in these areas. Accumulations are controlled by diluting the methane gas with fresh air delivered from the surface to the underground workings by powerful ventilation fans. Minimum quantities of air delivered to active and inactive areas are codified in the federal mining law (Code of Federal Regulations, 2009) and must be increased should the mining operation encounter elevated methane levels. However, the capacity of the surface fan facility and the size and extent of the underground workings are practical limitations that prevent delivery of ever-increasing quantities of fresh air to dilute elevated methane levels. Where ventilation alone is incapable of controlling these excessive methane emissions, supplemental controls

* Corresponding author. Tel.: +1 412 386 4008; fax: +1 412 386 6595.
E-mail address: cok6@cdc.gov (C.Ö. Karacan).

0166-5162/$ – see front matter. Published by Elsevier B.V.
doi:10.1016/j.coal.2012.04.002

such as degasification must be initiated. The successful application of these controls requires that the source of the methane gas first be identified.

This paper describes the identification of potential sources of excessive methane emissions at an underground coal mine that operates in a thin coal seam. Conduits for methane migration are examined and potential controls for these emissions are defined.

2. Location and description of the study mine

The study mine is a low-seam (~4 ft high) room-and-pillar mine located in Indiana County of Pennsylvania in the Northern Appalachian Basin (Fig. 1). Location of the mine is just outside of the Valley and Ridge Province of the Appalachian Plateau and is in the direction of decreased deformation (Fig. 1). Therefore, the study area was not affected severely by intense faulting, and folding occurred within the Valley and Ridge Province. However, due to the proximity of the study area to Allegheny Mountain Section (Fig. 1), the effects of tectonic forces on joints and joint patterns are still relevant within and around the mine location.

The mine operates in the Lower Kittanning coal seam and produces approximately 320,000 short tons of coal, on average, annually (MSHA, 2011). The average methane emission measured at the main return is approximately 160,000 scfd (standard cubic feet per day). Considering this average methane rate and the average annual coal production, the average specific methane emission from this mine is calculated as 182.5 scft (standard cubic feet per ton).

The ventilation fan delivers approximately 53,000 scfm (standard cubic feet per minute) fresh air into the underground workings. Methane concentrations and flow rates are monitored at multiple locations in return entries and at the working faces. Individual measurements at various locations within the mine usually show concentrations of carbon dioxide up to 0.15%, oxygen between 20.4% and 20.9%, and methane up to 0.3%. Although measured methane concentrations in the mine are lower than the statutory limit (<1%), increased methane emissions at the working faces are observed only when coal is being cut, but not when the faces are idle. This partly corroborates the observations of McCulloch and Deul (1973), who reported that the amount of gas emitted directly from Lower Kittanning coal into the mine workings was small. However, this does not explain why emissions drastically increase during mining of coal from the same face.

This study was conducted to explore the additional sources of methane observed in the mine, and the geologic and hydrodynamic factors that can be responsible for gas migration into the mine workings.

3. Depositional and structural geology of the region

3.1. Depositional setting

The Lower Kittanning coal, where the study mine is located, is one of the most extensively mined coals in Indiana and Cambria counties in Pennsylvania. The thickness of the Lower Kittanning coal ranges up to 5.5 ft, and there are only a few isolated areas indicating no coal. In places where there is minable coal thickness, it is not uncommon to have up to 4 ft of sandstone and shale associated with coal material. This pattern and varying thickness of partings in the coal is typically as a result of flooding of the peat swamp along the margins of the stream systems. In the study area, the immediate roof of the Lower Kittanning coal is composed of up to 7 in. of bone coal and up to 9 ft of dark, sandy shale. The immediate floor is about 4 ft of fire clay with coal and shale partings (Moore et al., 1976).

The main strata in the study area are deltaic and fluvial deposits of sandstones and shales (Fig. 2). The thickest sandstones were typically deposited in fluvial channels, which cut deep into the swamps, removing previously deposited sediments and coals. Shales and sandstones, which were deposited in brackish waters, compose a significant part of the lower half of the Allegheny Group. It is this part of the Allegheny Group where Kittanning Formation is present. Contrary to shales and sandstones, limestones and calcareous claystones were produced in freshwater lakes. These lithologies are more pronounced in the upper part of the Allegheny Group, and are overlain by Freeport coals (Skema et al., 2008).

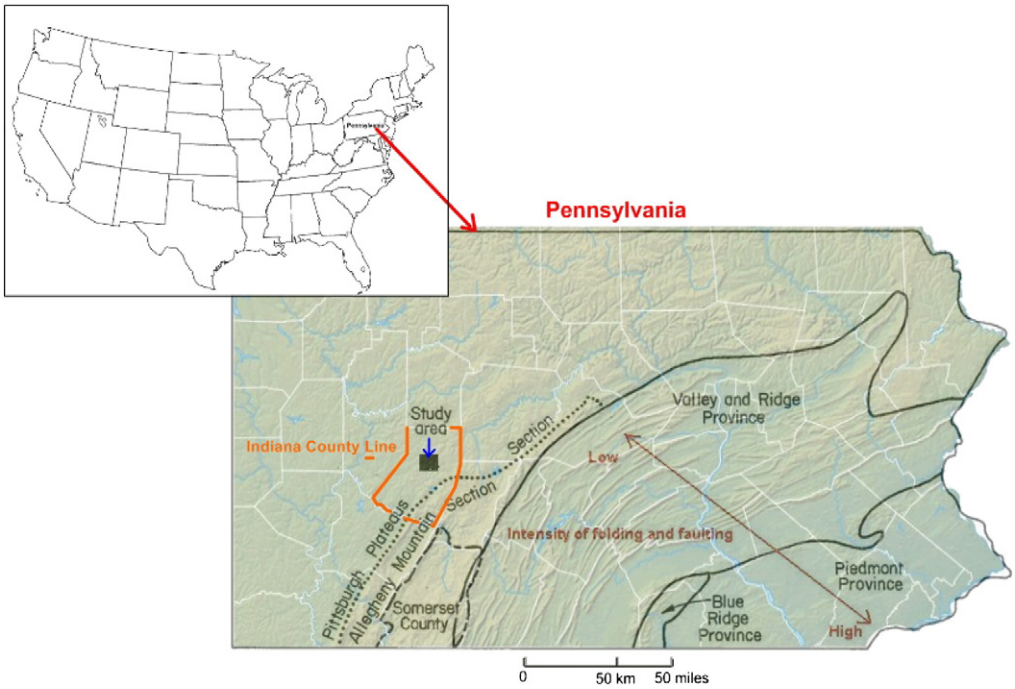

Fig. 1. Map of Pennsylvania with geologic deformations and various provinces due to Appalachian front development. Indiana County and the location of the study are shown in the map as well.

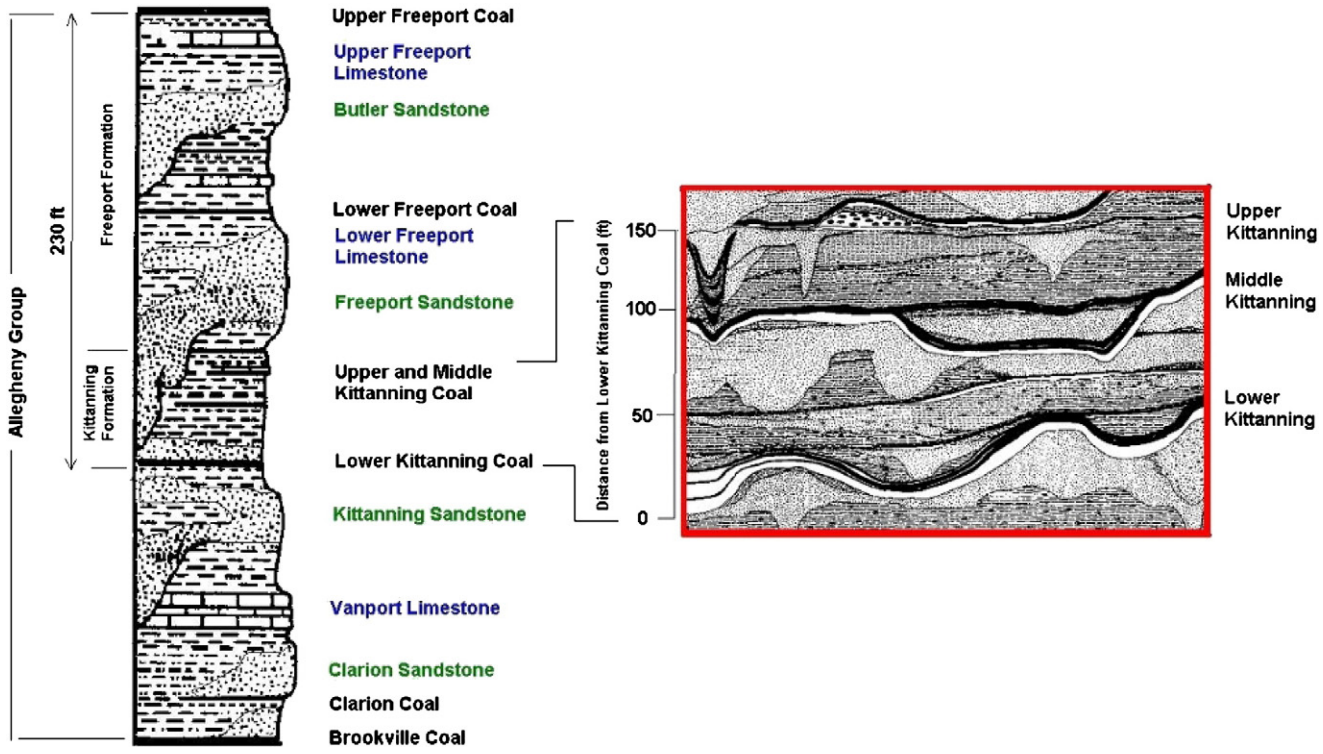

Fig. 2. Stratigraphic section of the Allegheny Group formations (Pennsylvanian system) showing locations of important coal and non-coal horizons. Right-hand picture shows complex depositional environment in Kittanning Formation and Kittanning coals.
(Modified from Kelafant et al., 1988).

The Kittanning coals have originated in peat swamps that were preserved with typically fine-grained mud. Kittanning coals formed on a coastal plain as a result of a sea advancing from the southwest. This process produced characteristically continuous coals of relatively uniform thickness covered by dark fossil-rich, siderite-rich, and pyrite-rich shales. By comparison, Freeport coals formed in peat swamps located at greater distances from the sea. Therefore, they were not affected by advancing seas, but were dissected more by rivers and freshwater lakes. In such a depositional environment, rivers deposited more sediment on portions of the peat swamps adjacent to the rivers with a discontinuous trend. Therefore, Freeport coals have more irregular surfaces and thicknesses compared to Kittanning coals.

The Lower Kittanning, Middle Kittanning, Upper Kittanning, Lower Freeport, and Upper Freeport coals of the Allegheny Group are the most prominent coals in this stratigraphy (Fig. 2). These coals are high-volatile and medium-volatile bituminous coals around the study area, and the approximate dividing line between these two ranks runs through Indiana County and very close to the location of study mine (Pennsylvania Geological Survey, 2011).

3.2. Structural features

Indiana County, Pennsylvania, is just outside of the Valley and Ridge Province of the Appalachian Plateau, where the most intense faulting and folding occurred on the southeastern edge of the plateau. This region is generally characterized by asymmetrical anticlines and synclines, which developed in the late Pennsylvanian to early Permian era (Berg et al., 1980). The dominant fracture and joint patterns in the Northern Appalachian coal basin tend to be oriented NW, which is a result of tectonic forces, associated with the Allegheny orogeny episode. The intensity of structural deformations generally decreases to the northwest direction (Fig. 1).

There are a number of different sections and provinces in the Plateau, as shown in Fig. 1. However, due to its proximity to the study area, the Allegheny Mountain section is probably most important for this study. In the Northern Allegheny Mountain section, which is closest to Indiana County and the study area, the general pattern of deformation due to folding is disrupted and it is not as severe as in the southern portion. The major folds in this area are the Chestnut Ridge anticline and the Laurel Hill anticline (Fig. 3A). The complexity of the depositional environment in the Kittanning and Freeport formations, and the structural deformation due to Allegheny orogeny, account for the extreme local and regional lithological variations, faults, and fractures in this area.

In addition to the major joint and fracture systems, the coal itself contains cleats, formed as a response to coalification and to local structural forces. Local structural forces are generally the major determinant of cleat density and orientation, which are important factors for directional permeability. In the Northern Appalachian basin, face cleats exhibit a strong NW–SE orientation (Kelafant et al., 1988) as shown in Fig. 3B.

3.3. Stratigraphy of the study area

Fig. 4 shows a general stratigraphic column of the study area described in Section 4. This figure indicates similar depositional character and rapid changes in formations discussed for Indiana County and shown in Fig. 2. In relation to roof stability and gas migration, depositional and structural character of the study area result in potential consequences for the mines operating in Kittanning and Freeport coals. The discontinuities and rapid changes in lithological features result in unstable roof conditions, and cracks and fractures that may extend to various overlying formations with a tortuous path. Iannacchione et al. (1981), who investigated the roof conditions in a mine operating in the Upper Kittanning coal, concluded that there were two distinct directional trends for unstable roof conditions; one trend was associated with the sandstone–shale transition zones, and the other with a fault system. The authors pointed out that the shale roof–rock interface had slickenside transition, which created

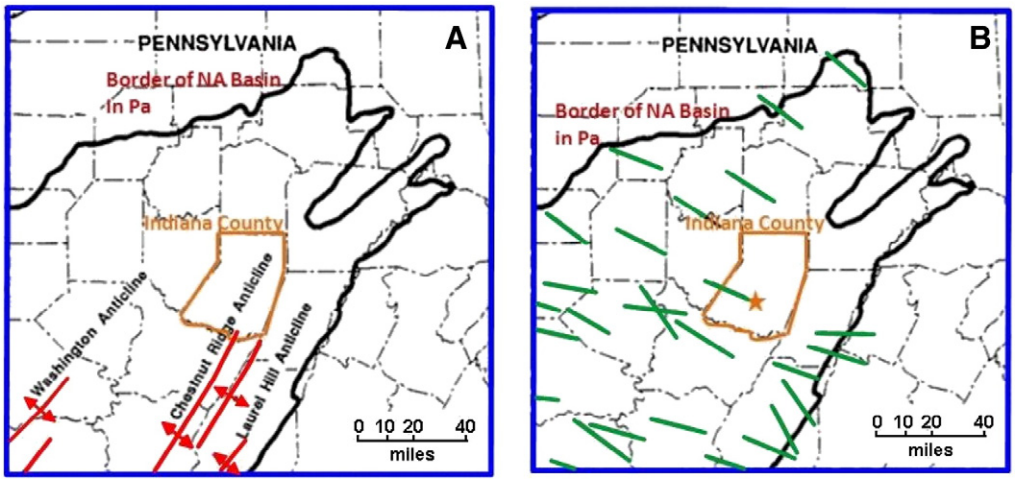

Fig. 3. Structure map (A) and dominant coal face-cleat direction (B) in and around Indiana County (modified from Kelafant et al., 1988). The heavy line that encompasses several counties in Pennsylvania is the border of Northern Appalachian coal basin in Pennsylvania. The "star" symbol is the location of the study mine in Indiana County.

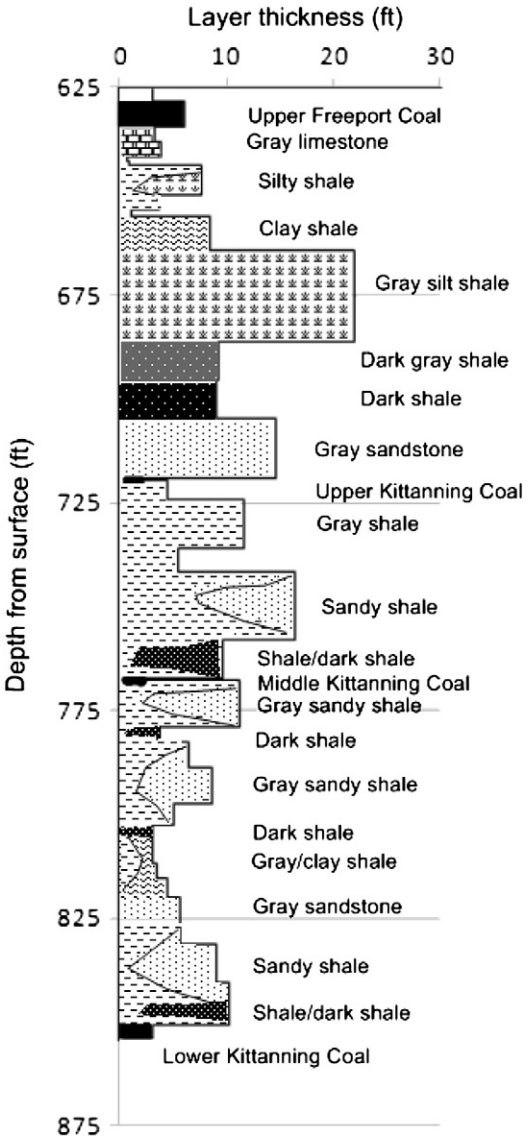

Fig. 4. General stratigraphic column of the formations and their thicknesses at the study site.

differential compaction that allowed the roof to be unstable. On the other hand, unstable shale roof–rock conditions that originated from faults were due to structural deformation of the strata. The observations revealed that these fractures and faults were smaller in comparison to those in the shale–sandstone transition zone. These deformations due to differential compaction and faulting can create fractures that can run through various lithological units during mining, thereby acting as conduits for available methane to migrate across various formations and into mine workings.

4. Study area, data sources, and measurements

In order to conduct a detailed analysis and modeling for this work, a study area was selected. The selected area included the active mine and portions of abandoned mines surrounding the active workings. In addition, it included groundwater monitoring and exploration boreholes, as well as the surface streams Two Lick Creek and Stoney Run, which could be important for groundwater recharge and discharge in the area (Fig. 5). The selected area was 17,100 ft in *easting* and 10,200 ft in *northing* directions.

The property line of the study mine in this area was bordered by a 15-year-old abandoned mine in the south and east directions. The study mine was also bounded in the east with the surface stream Yellow Creek. In addition to the abandoned workings shown in Fig. 5, it has been reported that there were some old abandoned mines in the overlying Freeport seams as well.

The area had 59 exploration boreholes that were drilled from the surface to the bottom of the Lower Kittanning seam. Information from these boreholes was used to compile surface elevation, depth, and thickness data of the Lower Kittanning seam and overlying shale formation. These data were used for geostatistical simulation and co-simulation purposes, which are discussed in Section 6. In addition to being used for compiling geological information, three of the exploration boreholes (GC Testings 1 to 3) were sampled for coals for gas content and permeability tests, and six of them (Obs Wells 1 to 6) were instrumented with piezometers to measure groundwater level and to sample groundwater for water quality analyses. The locations of all of the boreholes used in this study are shown in Fig. 5.

As part of regular coal evaluation and to assess the source of gas experienced in the mine, petrographic and compositional analyses, flotation analyses, gas content testing, and coal permeability

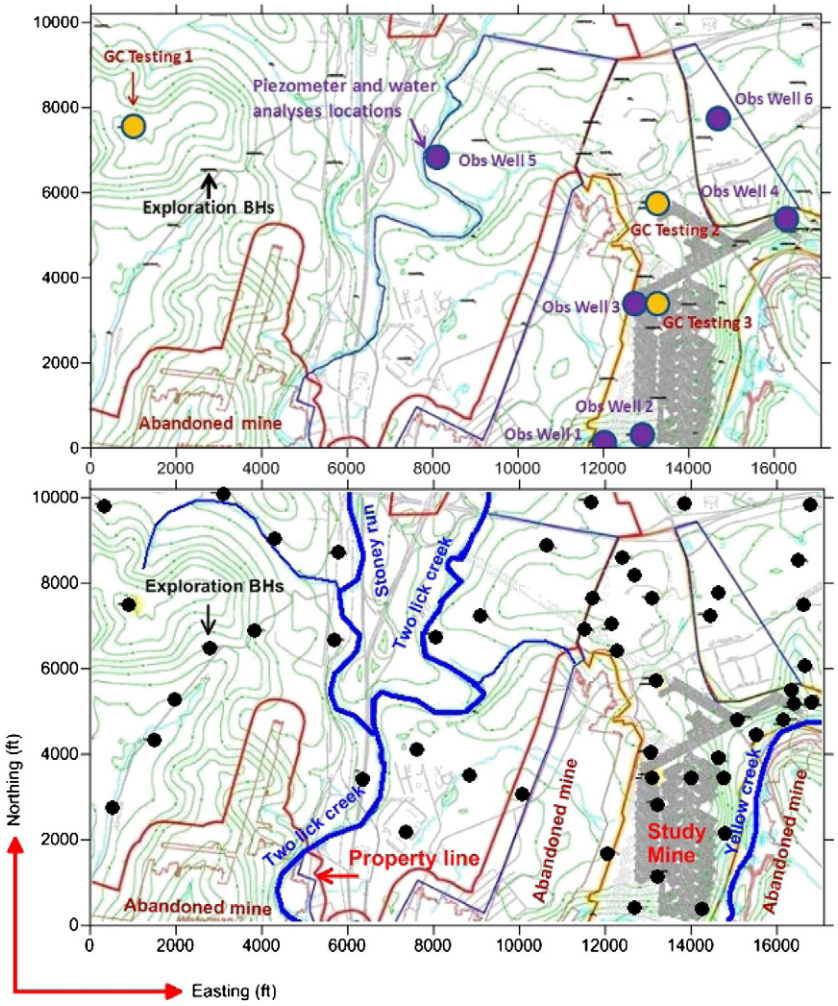

Fig. 5. Study mine and abandoned mines, various monitoring and data locations, and surface streams in the selected area.

measurement were conducted on coal samples taken from the boreholes and from the mine.

4.1. Proximate and petrographic analyses of Lower Kittanning coal

Proximate and petrographic analyses were performed on a newly cut coal sample taken from the mine to determine its composition and coal-utilization related properties. These tests showed that the coal sample had 24.7% volatile matter, 12.1% ash, and 63.2% fixed carbon. Sulfur content of the coal was 3.35% and the coal had a heat value of 13,785 Btu/lb. All these results are on a "dry" basis.

Petrographic analyses were performed on the same sample. These analyses showed that the sample had a mean maximum vitrinite reflectance (R_{omax},%) of 1.13 with a standard deviation of 0.0452. The results of petrographic analysis for maceral composition are given in Table 1.

4.2. Flotation results conducted on raw coals taken from exploration boreholes

As mentioned in Section 3.1, the Lower Kittanning seam can have a top bone coal in the study area due to depositional features. The thickness of this layer can be as much as 7 in. In order to quantify the influence of bone coal on coal quality and to in-place methane contents, flotation and coal quality tests were conducted and they were performed in two stages.

The first stage was sulfur, ash, and calorimetric tests on raw coal samples with the top bone coal included (WB) and after separating it from the main coal (WOB). These tests were performed on ~35 coal samples and basic statistics of the data were determined. Table 2 gives ash, sulfur, and heat value analyses of the coal samples. These results show that separating bone coal from raw coal samples decreased ash yield by about 6% and sulfur content ~0.5%, while

Table 1
Maceral composition (vol.%) analyses of Lower Kittanning coal sample.

Maceral composition (vol. %)			
Reactives	V-type	8	–
		9	0.8
		10	15.5
		11	58.8
		12	2.3
Vitrinite			77.4
Exinite			0.5
Resinite			0.0
Semifusinite			1.4
Total reactives			79.3
Inerts			
Semifusinite			2.6
Micrinite			9.2
Fusinite			1.1
Mineral matter			7.8

Table 2
Comparison of raw samples of Lower Kittanning seam retrieved from boreholes with (WB) and without (WOB) bone coal included, and the results of flotation tests with properties of recovered yields.

	Raw coal (WB)			Raw coal (WB) — float in 87.4 lb/ft^3 fluid				Raw coal (WB) — float in 93.6 lb/ft^3 fluid			
	Ash (%)	Sulfur (%)	Heat value (Btu/lb)	Yield (%)	Ash (%)	Sulfur (%)	Heat value (Btu/lb)	Yield (%)	Ash (%)	Sulfur (%)	Heat value (Btu/lb)
Mean	16.82	4.18	12,827.24	70.25	6.44	1.95	14,701.73	76.49	7.46	2.16	14,516.63
Median	17.09	4.12	12,755.00	69.98	6.37	1.91	14,700.00	77.85	7.46	2.18	14,535.50
Std dev.	3.06	1.05	510.85	4.55	0.99	0.27	169.24	5.05	0.91	0.31	152.61
Min.	9.11	2.49	11,872.00	58.76	4.87	1.45	14,192.00	65.74	6.00	1.61	14,102.00
Max.	22.55	7.63	14,057.00	78.43	9.68	2.55	14,956.00	84.53	10.16	2.84	14,737.00
Number of data	36	36	36	30	30	30	30	30	30	30	30
Mean	11.15	3.74	13,829.19	81.65	6.31	1.94	14,734.69	88.28	7.32	2.12	14,553.63
Median	10.90	3.65	13,876.00	82.36	6.31	1.91	14,750.00	88.51	7.22	2.19	14,597.00
Std dev.	1.89	0.92	333.62	3.98	1.00	0.27	173.51	3.39	0.91	0.29	159.46
Min.	8.58	2.04	12,930.00	72.69	4.84	1.45	14,192.00	81.75	6.03	1.59	14,102.00
Max.	16.42	5.80	14,277.98	86.45	9.68	2.48	14,976.00	93.89	10.17	2.63	14,784.00
Number of data	30	33	30	26	26	26	26	27	27	27	27

improving the heat value ~1000 Btu/lb, on average. Considering the thickness of bone coal in relation to total thickness of the seam, these results suggest that bone coal can contain a considerable amount of ash and thus decrease the heat value of the coal in general. Bone coal also increases the sulfur content of the coal seam.

The second set of tests was conducted to determine flotation yields of the Lower Kittanning coal using samples with and without bone, WB and WOB, respectively. The densities of the flotation mediums were 87.4 lb/ft^3 and 93.6 lb/ft^3 (1.4 and 1.5 g/cm^3, respectively). Flotation of raw coals, WB and WOB, in fluids with different densities helps improve the ash, sulfur, and heat value further. Table 2 shows the results of flotation tests and the properties of recovered yields. In addition, flotation decreased ash and sulfur contents while increasing the heat value significantly compared to the raw conditions presented in Table 1. However, using a heavier fluid in both cases increased ash and sulfur slightly in the recovered coal, while consequently decreasing the heat value, which can be attributed to making some of the high-ash and high-sulfur components float again in heavier medium.

4.3. Gas content testing of coal samples

In order to determine gas contents in the Lower Kittanning seam, desorption tests on six coal samples were conducted. Three of these samples were from core holes marked as GC Testings 1 to 3 in Fig. 5. The other three samples were from different locations within the mine.

For desorption testing, direct-method of measurement (Diamond and Levine, 1981) was used. Since gas content of the coal might be different at different heights of the seam due to compositional variations in coal, full coal cores retrieved from boreholes were separated into 3 samples as the top (bone coal), middle, and bottom. These samples were placed in canisters and tested separately.

Desorbed methane volumes were measured in the field for nearly 2 h as frequent as possible after the samples were placed in the canisters. Estimates of lost gas prior to sealing the samples in canisters were calculated based on the readings taken during the first 2 h of desorption. This is a standard procedure that involves linear extrapolation of initial readings to time “zero”. After initial desorption of samples in the field, the canisters were taken to the laboratory where the rest of desorption testing was continued for 3–4 months under controlled temperature conditions at ~70 °F.

During desorption tests, temperature and atmospheric pressure were also recorded with each reading of the gas volume so that all volume readings could be converted to standard temperature and pressure (STP) conditions. Desorption tests were continued for at least 20 days or until the readings were stable. Fig. 6 shows desorption kinetics of all tested coals with their sampling locations.

The results shown in Fig. 6 indicate that the in-mine samples had low desorbed methane contents. The value of gas contents reached only 40–50 scft after 20 days. This is likely due to exposure of the in-mine samples to the mine atmosphere long enough to lose most of their gas content prior to testing. Interestingly, gas contents of these samples were very close to the gas contents of the top bone coal samples separated from borehole coal cores (GC Testings 1 to 3 locations — Fig. 5). Low gas contents of bone coals can be attributed to their high-ash content as discussed in the previous section. Thus, owing to the high ash and low gas contents, bone coal is not expected to contribute a lot to the methane emissions experienced during mining.

Desorbed gas contents of the middle and bottom samples of the same cores obtained from boreholes, however, were significantly different. This is most likely due to the compositional differences of these samples compared to top bone coals. The desorption data shown in Fig. 6 indicate that the middle and bottom samples from GC Testing 1 location had a very high (~270 scft) gas content, followed by those of GC Testing 2 location (~100 scft). Measured gas contents of GC Testing 3 location were lowest, possibly due to its proximity to the active workings (Fig. 5). Gas desorption data not only indicate the amount of gas, but also its kinetics during the desorption process. Comparison of the slope of desorption data of various samples suggests that the coal at GC Testing 1 location desorbs faster than the coal at the other two locations.

The gas amount that was not released during desorption period was referred to as residual gas. Residual gas of desorbed cores was determined by crushing the coal samples in the sealed canisters using ball-and-mill method. Residual gas content determination was conducted on all samples following the desorption tests. Table 3 gives separate gas content amounts (desorbed, lost, and residual) of coal samples and their depths at the corresponding sampling locations.

4.4. Coal permeability measurement

Permeability measurement of the Lower Kittanning coal sample was conducted at Southern Illinois University, Carbondale, using a triaxial core flooding system. A cylindrical core 3 in. in diameter and 4.2 in. in length was drilled from a block of coal that was retrieved from the mine. The core was preserved to prevent any damage due to weathering and oxidation by storing it in an environmental chamber with no source of light and under controlled conditions of temperature and humidity.

Since coal permeability is sensitive to stress conditions, special attention was given to replicate the in-situ stresses by controlling external stresses and gas pressure during experiments. In order to achieve this, the experimental setup was instrumented with independent controls and monitors of horizontal and vertical stresses, axial

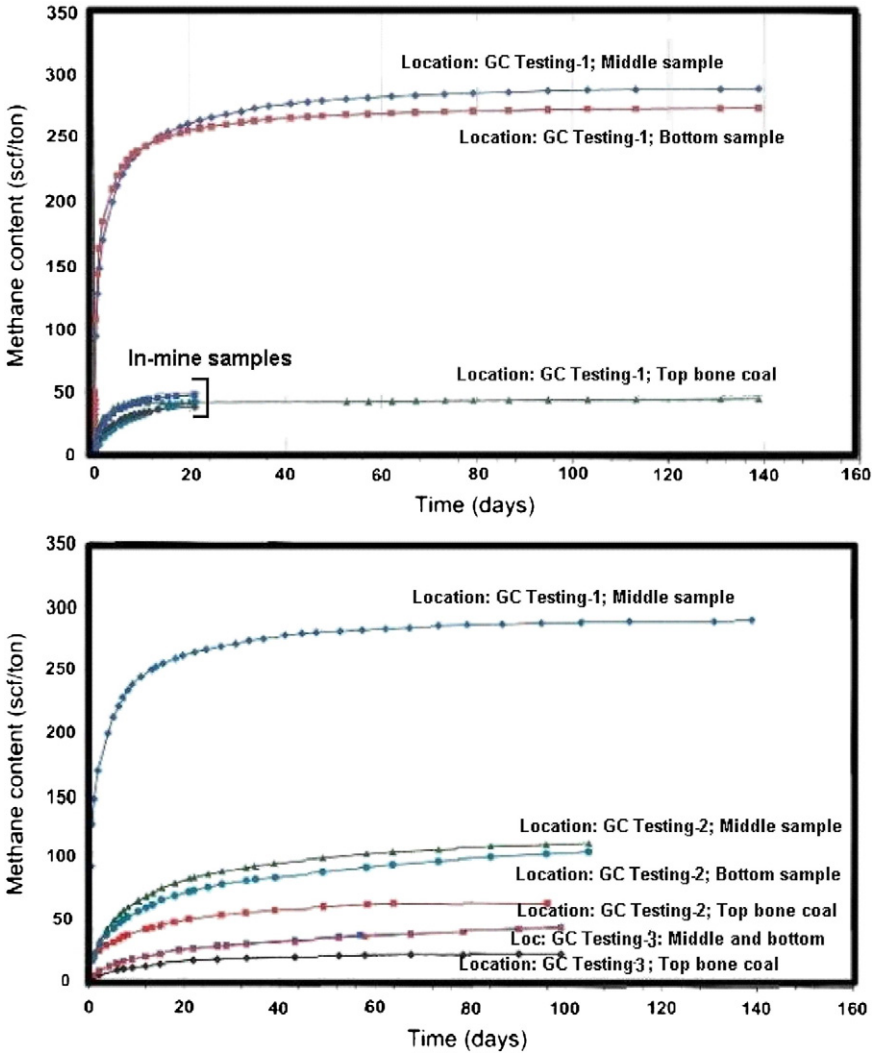

Fig. 6. Desorption tests conducted on various coal samples recovered from boreholes: GC Testings 1 to 3 (Fig. 5) and on coals taken from the mine.

and radial strains, upstream and downstream gas pressures, and temperature.

The experimental setup consisted of a triaxial cell, a circumferential extensometer to monitor and control shrinkage and swelling of the core, two linear variable differential transducers (LVDT) attached directly to the sample to monitor changes in its length, a loading system, and devices to measure methane flow rate.

For the sample depth of 450 ft at the mine's location, the in situ vertical stress (σ_v) and horizontal stress (σ_h) were estimated to be ~450 psi and ~340 psi, respectively. Once mechanical equilibrium of the sample under these conditions was achieved, the sample was flushed with helium. Methane was then injected in a step-wise manner to a final average pore pressure of ~170 psi, and the flow rate under a small pressure gradient was measured at the downstream end. Permeability was calculated using a modified Darcy equation for compressible flow. A similar procedure was applied by reducing the horizontal stress to ~200 psi. The latter was aimed to see if there could be a significant increase in permeability as a result of mining-induced stress reduction. The experimental conditions and calculated permeabilities are presented in Table 4.

The permeability values reported in Table 4 are generally high for coal permeabilities. This particular sample had well-developed cleats and came from a shallow depth. Thus, the measured permeabilities are not entirely unexpected. However, even determined under in-situ stress conditions, coal permeabilities determined in the laboratory are usually questionable as they are typically much higher than in-situ permeabilities and thus they should be treated with caution. Regardless, as noted earlier, the mine did not experience emissions at high rates from idle faces and the gas was released at sufficient quantities only when the coal broke away from the seam. One possible explanation for this problem may be the high water saturation within cleats, which reduced gas flow by decreasing relative permeability to gas. When the coal block was broken from the coal face and cleats were subjected to high pore pressure reduction

Table 3
Locations of coal samples that were tested in canisters and their gas content values.

Location	Sample	Depth (ft)	Total gas (scft)	Desorbed gas (scft)	Lost gas (scft)	Residual gas (scft)
GC Testing 1	Top	850	56	48	5	3
	Middle	850	325	291	23	11
	Bottom	850	318	275	34	9
GC Testing 2	Top	400	75	66	7	2
	Middle	400	120	114	4	2
	Bottom	400	126	107	4	15
GC Testing 3	Top	438	29	26	1	2
	Middle	438	50	47	1	2
	Bottom	438	53	48	1	4
In-mine	Rib	–	61	38	6	17
	Loader	–	59	48	4	7
	Cross-cut	–	66	43	1	22

Table 4
Experimental stress conditions and calculated permeabilities.

Vertical stress (psi)	Mean pore pressure (psi)	Horizontal stress (psi)	Permeability (md)
445	167	351	3.34
447	170	212	3.40

gradient, on the other hand, the high gradient potentially mobilized gas and water out from the coal cleats. Therefore, hydrodynamics of this area could be playing a significant role in gas flow and for the emissions experienced in the mine.

4.5. Piezometric measurements of groundwater levels and geochemistry of water samples

As a first approximation, direction of water flow and the potential level of contaminant transport from abandoned mines do not necessarily indicate accompanying methane migration from these abandoned workings. In fact, the United States EPA (2004) shows that the mines that are flooded cease emission of any methane after 8–10 years of abandonment. Since the abandoned workings surrounding the active mine in this study are much older than 8–10 years and are known to be flooded, this rules out methane emissions into the active workings from the abandoned mines in the Lower Kittanning seam.

Temporal variations and overall magnitudes in groundwater levels and geochemical compositions are important in this area, which has multiple surface streams (Fig. 5) that are likely in connection with the groundwater system (Bencala, 2011) in the Lower Kittanning coal and in the overlying strata. Since overlying coal-bearing strata contain the Middle and Upper Kittanning seams and the Freeport seams within a 200–250 ft interval, which are known to be gassy (Diamond et al., 1992) and contain voids of abandoned mines, the groundwater conditions can be particularly important.

Both coal-bearing formations and abandoned mines are known to affect the quality of groundwater. The discharges from these sources are usually characterized as acid mine drainage, due to the low pH and high dissolved metal contents (Al, Mn, etc.). Pyrite (FeS_2) and other sulfide minerals, which are usually finely dispersed in coal, both in coal-measure rocks and in abandoned mines, are known to be the source of acidic waters. Oxygen entering pyrite-rich environments is usually consumed through sulfide and the iron oxidation

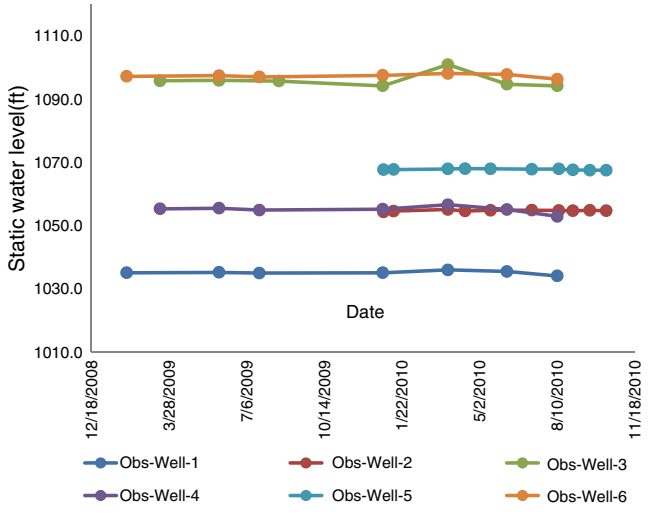

Fig. 7. Temporal changes in groundwater level measured at different observation locations.

Table 5
Basic statistical data of temporal quantities measured in groundwater observation wells (Obs Wells 1 to 6).

Parameter	# of data	Min.	Max.	Mean	Std. dev.
Fe (mg/l)	6	0.15	45.33	9.81	17.47
Suspended solids (mg/l)	6	3.42	91.00	28.39	32.16
Mn (mg/l)	6	0.01	0.70	0.35	0.30
Al (mg/l)	6	0.08	3.75	0.80	1.45
SO_4 (mg/l)	6	5.43	47.86	25.52	14.71
Conductivity (μmho)	6	185.57	1071.29	452.98	311.49
Alkalinity (mg/l)	6	43.00	359.56	164.96	104.36
Acidity (mg/l)	6	−339.15	−35.66	−151.48	100.07
pH	6	6.51	8.09	7.16	0.54
Static water level (ft)	6	1035.2	1097.4	1067.8	24.7

reactions catalyzed by bacteria (National Research Council, 2006). In addition, carbonates with siderite may add additional iron to underground waters and discharges emanating from them (Banks et al., 1997). At low pH values, 19 mol of acidity is generated for every mole of FeS_2 oxidized due to reactions with pyrite and Fe^{3+} as shown below (Worrall and Pearson, 2001):

$$FeS_2 + 14Fe^{3+} + 8H_2O \rightarrow 15Fe^{2+} + 2SO_4^{2-} + 16H^+ \quad (1)$$

$$Fe^{3+} + 3H_2O \rightarrow Fe(OH)_3 + 3H^+ \quad (2)$$

In reality, the pH of the water emerging from coal-bearing strata can be generally close-to-neutral due to neutralizing and buffering effects of limestones, quartz, feldspars, and clays. The duration of acid generation and neutralization depends on the amount of pyrite, microbial community, oxygen amount, buffering minerals, as well as residence times and hydraulic properties of the strata. It is suggested (Younger, 2000) that after flooding of an abandoned mine is complete and groundwater begins to migrate from the mine voids into surface waters or to adjoining aquifers, flushing the mine voids with fresh water results in a gradual improvement in the quality of groundwater mainly by decreasing iron levels and by stabilization of pH around 7. However, these processes are highly site-specific within a certain region. Therefore, it is important to conduct sampling studies for a more accurate evaluation.

At this mine site, six of the exploration boreholes (Obs Wells 1 to 6, in Fig. 5) were equipped with piezometers to monitor temporal variations in groundwater level. Water samples were also collected from these boreholes to evaluate their quality by geochemical analyses. For this work, iron (Fe), manganese (Mn), aluminum (Al), sulfate (SO_4), suspended solids, alkalinity, acidity (all in mg/l), pH, and specific conductivity (μmho) were measured or calculated.

Fig. 7 shows the temporal data for groundwater level. This figure shows that the groundwater level at observation locations were within a general 100-ft interval. However, the measurements did not show drastic temporal variations. This may be attributed to either very steady precipitation in the area throughout the monitoring period, or almost constant recharge and discharge rates regardless of the precipitation frequency and amount. Although almost-constant water levels may not be directly indicative of water quality, they are a good indication of the existence of a constant water head and flow gradient which can be used to predict water flow direction within the study area.

Water samples were also taken and analyzed at the same times as the water level measurements, though sampling frequency was insufficient to reveal a conclusive trend in water quality changes. Therefore, temporal data of each measured quantity from these boreholes were averaged to assign a single value to the spatial locations of the observation wells. This approach was implemented to apply geostatistical modeling for the assessment of water level and of

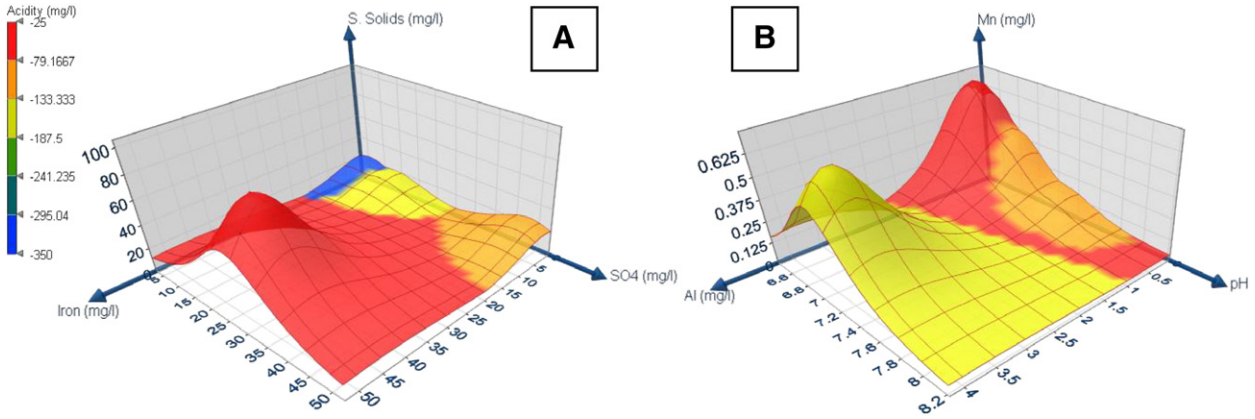

Fig. 8. Relationship between Fe, SO_4, suspended solids and acidity level (A), and Mn, Al, pH and acidity level (B).

some of the water quality attributes within the study area. Table 5 shows the basic statistical data that resulted from averaging of temporal quantities.

Averaging temporal measurements at their corresponding spatial locations also enabled interpretation of relationships between various attributes in this area. For instance, Fig. 8A and B show three-

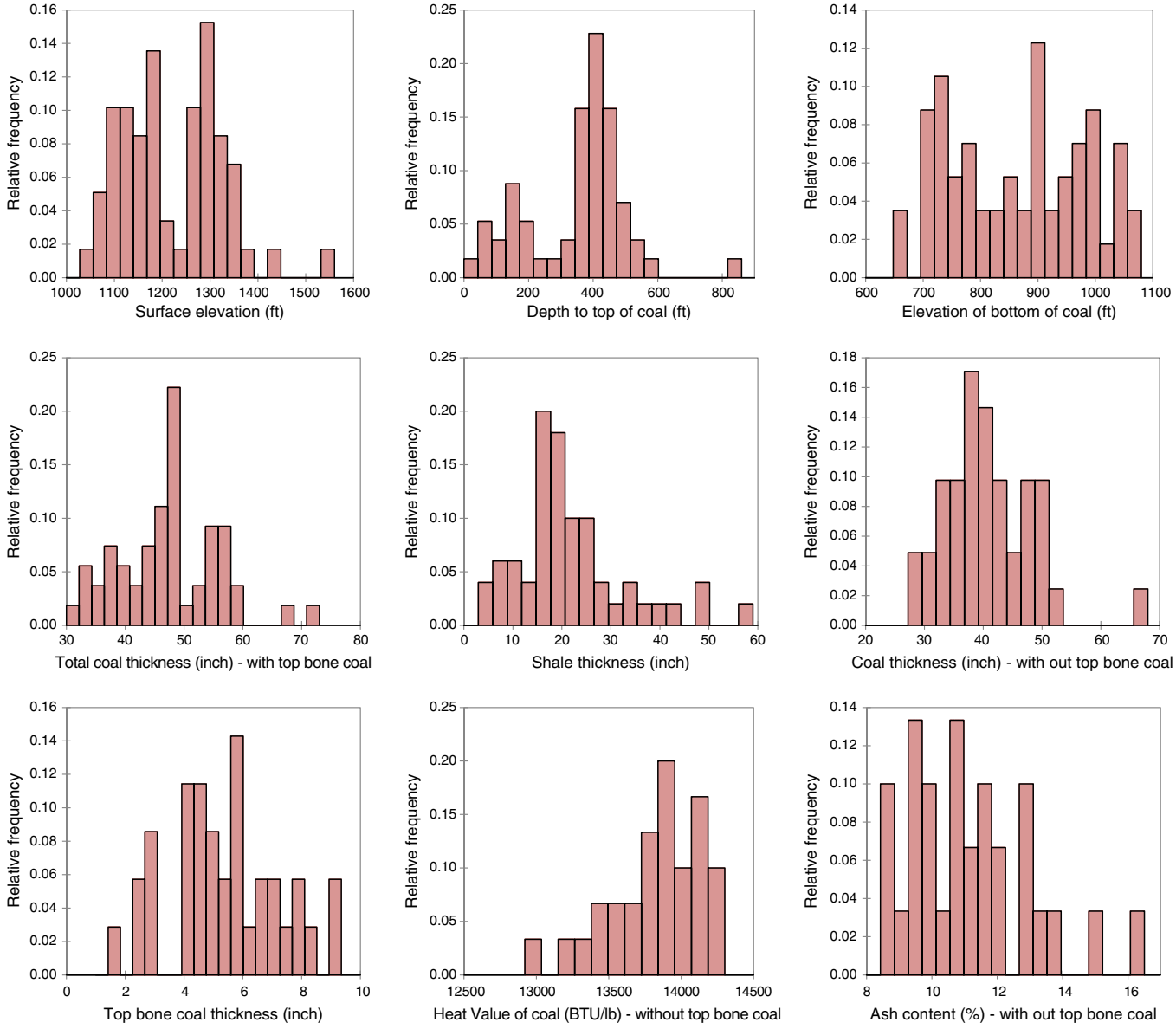

Fig. 9. Distributions of various attributes obtained from exploration boreholes shown in Fig. 5.

Table 6
Basic univariate statistical measures of the data obtained from exploration boreholes.

Variable	# of data	Min.	Max.	Mean	Std. dev.
Surface elevation (ft)	59	1043.50	1555.00	1222.02	105.24
Depth to top of coal (ft)	57	39.00	850.67	351.72	155.28
Elevation of bottom of coal (ft)	57	648.98	1073.50	866.29	120.34
Total coal thickness (inch)	54	30.00	72.00	47.37	8.57
Shale thickness (inch)	50	3.75	58.00	21.81	11.63
Coal thickness (inch)	41	29.00	67.00	40.87	7.63
Top bone thickness (inch)	35	1.50	9.25	5.39	1.92
Heat value of coal (Btu/lb)	30	12,930.0	14,277.9	13,829.2	333.6
Ash content of coal (%)	30	8.58	16.42	11.15	1.89

dimensional plots of various attributes based on these 6 data points. Fig. 8A shows that at a Fe content of ~40 mg/l and SO_4 content of ~30 mg/l, concentration of suspended solids (S. Solids) was highest at ~80 mg/l. At these values, acidity of the water was ~25 mg/l. This figure shows that acidity decreased when Fe was below 20 mg/l and SO_4 was below 25 mg/l. Fig. 8B, on the other hand, compares Al, pH, and Mn levels and the acidity levels with which they are associated. This figure shows that the highest Mn levels (~0.6 mg/l) were associated with pH levels of <7, and occurred at the low and high ends of Al concentrations. Depending on the level of Al, however, acidity of groundwater might be different — i.e. higher at lower Al levels.

4.6. Raw data obtained from exploration borehole drilling program

The study area comprised 59 exploration boreholes, all of which were drilled to the bottom of the Lower Kittanning coal and provided information about attributes such as elevations, depths, and thicknesses of coal, top bone coal, and shale in the immediate roof of the Lower Kittanning seam. Coal samples retrieved from these boreholes were analyzed and provided spatial information on heat and ash contents. The data from exploration boreholes were used in area-wide predictions of these attributes using geostatistical techniques. Fig. 9 shows the histograms of different attributes obtained from exploration boreholes. Table 6 gives the basic univariate statistics of the data shown in these histograms.

In addition to the raw data obtained from exploration boreholes, analyses of heat and ash contents were further used in MCP 2.0 (Karacan, 2010), first to predict and verify the gas content data given by desorption testing (Table 3), then to predict total gas content of the Lower Kittanning coal at various spatial locations. The values calculated using MCP 2.0 presented a bi-modal distribution (Fig. 10) with 77 scft, 280 scft, 165 scft and 53.8 as minimum, maximum, mean, and standard deviation, respectively. The observed bi-model distribution of total gas content data can be due to the changing rank of the coal within the study area. The total gas content data, along with other information such as coal depth, thickness, ash content, and density were used to geostatistically calculate in-place gas amount within the study area using the technique presented in Karacan et al. (2012). Geostatistical analysis and modeling of in-place gas amount in the Lower Kittanning seam in the study area will be presented and discussed in Section 5.

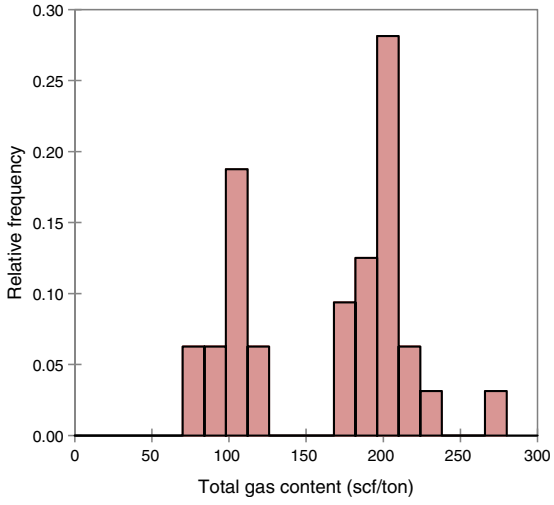

Fig. 10. Histogram of total gas content values predicted for Lower Kittanning coal at the study area using MCP 2.0.

5. Statistical and geostatistical analyses and modeling

5.1. Principal component analyses (PCA) of water quality data with structural data from exploration boreholes

In this study, principal component analyses (PCA) were used to evaluate the relationships of water quality data with some of the attributes from exploration boreholes. For this purpose, water quality data —Fe, Mn, Al, SO_4, suspended solids, alkalinity, acidity, pH, and specific conductivity—were combined with coal depth, coal top elevation, shale thickness, surface elevation, water level, and water head data measured from the boreholes at the same spatial locations. The water level and water head data represent the groundwater flow and saturated thickness above the Lower Kittanning coal, respectively. Identifying principal components within these data reduces the dimensionality of the data set, while retaining as much of the variance as possible.

Most of the variance in the data set is retained in the first few principal components. Elimination of principal components that do not contribute to the variance of the data decreases the dimension of the data set, while revealing information on correlations between

Table 7
Variability carried by different principal components and factor loadings of variables within these components after Varimax rotation. Bold numbers indicate significant variables in each principal component.

	F1	F2	F3
Variability, %	34.484	22.999	21.915
Cum. variability, %	34.484	57.484	79.399
Factor loadings			
Variables	F1	F2	F3
Fe	0.422	0.079	0.096
Suspended solids	0.174	−0.139	0.239
Mn	0.663	**0.651**	0.037
Al	0.194	**0.891**	−0.097
SO4	0.547	0.082	**0.790**
Conductivity	−**0.968**	0.034	−0.193
Alkalinity	−**0.947**	−0.050	−0.196
Acidity	**0.947**	0.002	0.202
pH	−**0.945**	−0.125	−0.068
Coal depth	0.283	0.327	**0.739**
Coal top elevation	0.104	−**0.974**	−0.155
Shale thickness	0.122	−0.348	−**0.897**
Surface elevation	0.387	−0.364	**0.634**
Water level	0.553	0.042	**0.754**
Water head	0.046	**0.933**	0.344

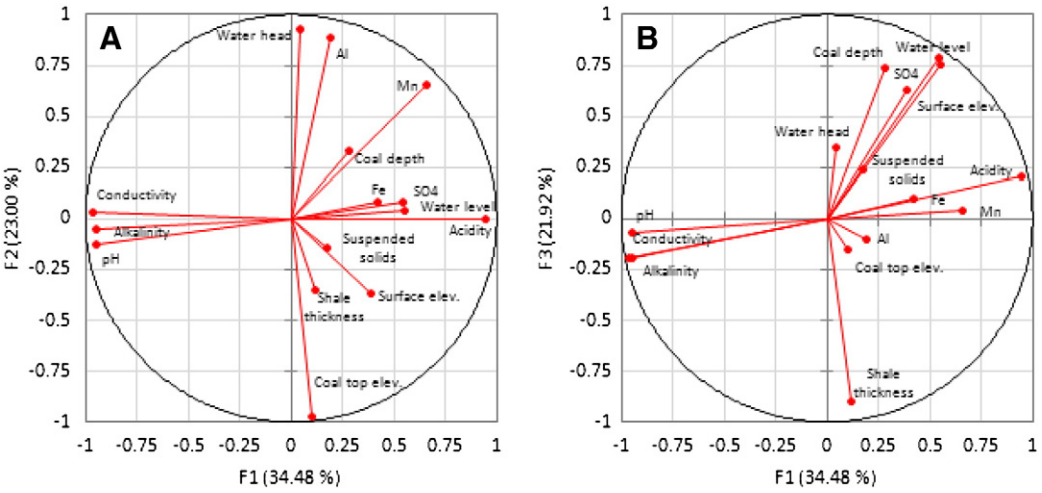

Fig. 11. Factorial space plots on 1st (F1) and 2nd (F2) and 1st (F1) and 3rd (F3) principal components.

variables and their weights in corresponding principal components. PCA component analyses have been used before in different studies related to gas management in coal mines (e.g. Karacan, 2008, 2009). In order to improve interpretability of PCA results in this study, Kaiser's varimax rotation technique, in which component vectors are rotated to a position so that the sum of the variances of the loadings would be a maximum, was used and presented.

Table 7 shows the variation and cumulative variation within the data set based on the rotated matrix. This table shows that almost 80% of the variance can be represented by the first 3 components. Furthermore, this table also shows how the variables are separated between columns according to the properties that they represent.

Table 7 shows that the first principal component is related to the acidic/alkaline nature of groundwater. The pH, conductivity, acidity, and alkalinity are main variables with highest factor loadings in this principal component. Acidity, however, is correlated with others negatively due to its negative sign. The second principal component represents Al and Mn and the structural properties, i.e. coal top elevation and water head. These two ions are positively correlated with water head (saturated formation thickness) and negatively correlated with coal top elevation. Thus, Al and Mn seem to be concentrated at deeper zones of the area. The third principal component is weighted more by the exploration borehole data included in this analysis and with sulfate content. In this component, coal depth, surface elevation, water level, shale thickness, and sulfate are important, although shale thickness is negatively correlated with others. Thus, while sulfate levels seem to be more impacted by depth and water level, they do not seem to positively correlate with the thickness of shale overlying the Lower Kittanning seam.

Fig. 11 presents factor loadings and the relationships of various parameters. Fig. 11A shows that pH, conductivity, and alkalinity are related to each other and negatively correlated with acidity, water level, SO_4, and Fe. The central positions of water head and coal top elevation on the 2nd principal component, with respect to the 1st principal component, signify absence of their effects on these variables. Therefore, water level, and thus the direction of flow, has more influence on the acidic nature of groundwater and Fe and SO_4 quantities. Fig. 11B indicates that local shale thickness does not have any influence on Fe and acidity, suggesting that local shale thickness in this area is not related to the acidity and Fe measured in groundwater. However, Fe and acidity being along the same direction can indicate an acidity-forming path as shown in Eqs. (1) and (2), and may suggest that pyrite in overlying coals and coal-bearing formations can be the source of acidity and Fe.

These observations related to water quality and their relation to water level and water head are important since they may indicate that the source of methane in active mines can also be overlying formations (at least partially in addition to the in-place methane in the Lower Kittanning seam) and that methane may be carried by groundwater in the direction of active workings. Thus, water level and water head not only show changes in groundwater quality but also the potential flow direction of methane with groundwater. Furthermore, water head also shows the thickness of the saturated zone that potentially covers methane-rich formations, such as coal seams, that may be the source of methane emissions. The cracks along slickensides between shales and sandstones and other fractures due to structural deformation of this area, as discussed in previous sections, could be the paths of groundwater and methane flow. However, structural complexities of Allegheny Group formations and coal seams make it difficult to determine exact directions of water flow and water head, particularly with only 6 spatial measurements within the entire study area. A similar conclusion was made by Harper and Olyphant (1993), who attempted to evaluate recharge and hydrologic conditions in the vicinity of abandoned coal mines around Cannelburg, Indiana. Therefore, water level and some of the monitored water quality attributes were geostatistically co-simulated with exploration borehole data to predict groundwater flow direction and water head distribution in the entire study area, with the understanding of potential methane migration into active workings.

Table 8
Summary of parameters that describe analytical semivariograms for overburden depth, coal thickness, and ash and gas content attributes of the Lower Kittanning seam at the study area. All semivariograms were analyzed using normal-score data and were described with a one-nested structure.

Lower Kittanning coal	Overburden (ft)	Thickness (inch)	Ash (%)	Total gas content (scft)
Model	Gaussian	Spherical	Spherical	Exponential
Nugget	0.05	0.25	0.01	0.01
Sill	0.95	0.65	0.90	0.95
Maximum range	5742	2150	4050	5920
Medium range	5244	1900	3870	5680
Minimum range	5016	1800	3780	5440

5.2. Geostatistical analyses and modeling

Geostatistics and geostatistical modeling techniques are used to determine values at unsampled locations. Thus, they are unique methods to establish spatial correlations in sampled data to form continuity and to assess the uncertainty of the attributes that are being investigated.

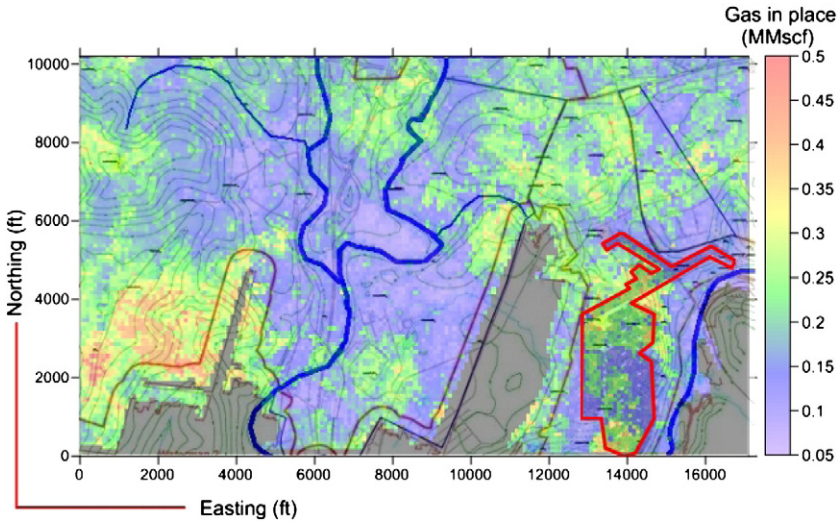

Fig. 12. Q50 gas-in-place realization for the study area. In this figure abandoned mine areas were blanked with gray color and the active mine was outlined with red.

Geostatistical analyses and modeling techniques, some of which are described in detail in Webster and Oliver (2007), Leuangthong et al. (2008), Deutsch and Journel (1998), Remy et al. (2009), Olea (2009), and Wackernagel (2010), have been widely used for geological, environmental, mining, and petroleum engineering. For instance, Olea et al. (2011a) presented a methodology using geostatistical approaches to quantify the uncertainty in coal resource assessments, applying the technique to a Texas lignite deposit. Heriawan and Koike (2008) identified spatial heterogeneity and resource quality of a coal deposit in Indonesia using geostatistics. They also correlated the distribution of various elements within the coal using multivariate geostatistics. Hindistan et al. (2010) used kriging as a tool to predict and control coal quality during longwall mining so that produced coal would comply with certain product specifications. Besides many other techniques, geostatistics has been used to assess spatial uncertainty of soil water content (Delbari et al., 2009) and to explore the spatial relations between soil physical properties and electrical conductivity (Carroll and Oliver, 2005) and to assess flow impacted by structural control in a karst aquifer (Valdes et al., 2007).

In this work, geostatistics and geostatistical modeling techniques were used to evaluate in-place gas amounts in the Lower Kittanning seam, and to assess hydrodynamics and groundwater quality that could impact methane emissions in the study mine. The data used in geostatistical modeling were obtained from 59 exploration boreholes and 6 monitoring locations shown in Fig. 5. For modeling this area, the data were assigned to a 172×102 Cartesian grid in which each grid was 100 ft in the x-direction and 101 ft in the y-direction. These grid dimensions result in ~1/4th of an acre in area per model grid.

The Stanford University Geostatistical Modeling Software (SGeMS) was used for spatial correlation analyses and for stochastic sequential Gaussian simulations and co-simulations (Remy et al., 2009). Sequential Gaussian simulation (SGSIM) and co-simulation are semivariogram-based techniques that take advantage of properties of Gaussian random functions (e.g. Gómez-Hernández and Cassiraga, 1994). Therefore, the input data should be transformed to normal-score space, if they are not perfectly Gaussian, prior to semivariogram analyses and simulations. Since none of the distributions from exploration boreholes were Gaussian (Fig. 9), data transformations were made prior to analyses, with these transformations reversed after simulations were performed.

5.2.1. Geostatistical modeling of in-place gas content of Lower Kittanning seam

Lower Kittanning coal's gas-in-place in the study area was computed based on only the gas-rich coal thickness. Thus, the thickness of bone coal and its ash and gas content were not included in this calculation. Excluding bone coal from gas-in-place calculation was not expected to cause a significant difference in gas amounts, since bone coal is relatively thin in the entire study area (Fig. 9) and has

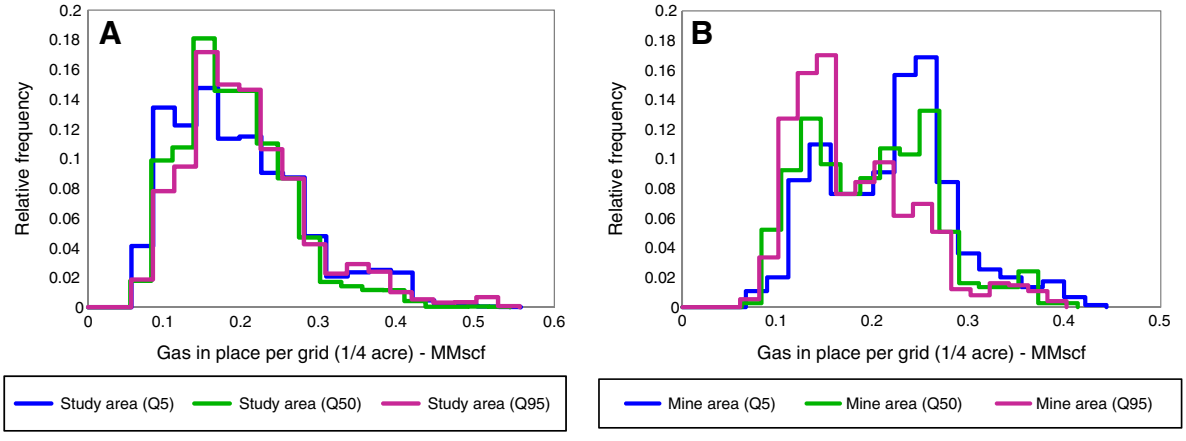

Fig. 13. Gas-in-place histograms for Q5, Q50, and Q95 for the entire study area (based on 17,544 grids) (A) and for the mine area (748 grids) (B) outlined in Fig. 12.

Table 9
Correlations between normal score values of acidity and water level with surface elevation data (NS refers to normal score values) based on 6 values from observation wells.

	Acidity–NS	Surface elev.–NS	Water level–NS
Acidity–NS	1	**0.764**	0.565
Surface elev.–NS	0.764	1	0.776
Water level–NS	0.565	**0.776**	1

high ash and low gas contents, as discussed in the coal analyses sections. Also, total gas contents were calculated using MCP 2.0, and they could be used directly for semivariogram modeling in volumetric gas-in-place calculations.

In-place methane amount was computed by following essentially the same procedure and method described in Karacan et al. (2012). Therefore, the details of these analyses and computations will not be discussed again in this paper. Semivariograms were modeled in multiple directions on the normal-score data following Olea (2006). Directional experimental semivariograms of normal scores were searched in each case, with 0°, 45°, 90°, and 135° starting from the north and changing towards the east direction of lag vectors. The lag separation distances were generally between 150 and 500 ft, with 75–250 ft lag tolerances, and a tolerance of azimuth was defined as 22.5° with bandwidths of approximately 2500 ft. Since the modeling of semivariograms showed no significant anisotropy, the isotropic modeling approach was adopted. The parameters of analytical semivariograms representing the normal-score data of coal thickness, overburden depth, ash content, and total gas content are given in Table 8.

For each attribute, 100 realizations, which can be seen as numerical models of possible distribution of the simulated property, were generated. Simulated realizations were compared with the measured data through Q–Q plots to determine if they produced linear trends indicative of representative simulations. These 100 realizations, each of which included 17,544 grid data, were ranked based on the cumulative gas-in-place values to determine the realizations corresponding to 5% (Q5), 50% (Q50), and 95% (Q95) quantiles. In this work, only 50% quantile (Q50) realizations were used for visualizations, whereas Q5 and Q95 were given with their histograms, as needed.

Fig. 12 shows the Q50 realization of the gas-in-place map, which was overlaid with the map of the study area. This figure shows that the area has in-place gas contents ranging from 0.05 MMscf (one million standard cubic feet) to 0.5 MMscf per grid (~1/4 acre). It is noticeable that the stream basins have lesser amounts of gas compared to the rest of the area. The gas-in-place values for the entire area corresponding to Q5, Q50, and Q95 were 2867 MMscf, 3174 MMscf, and 3442 MMscf, respectively. Grid value distributions for these values are given in Fig. 13A.

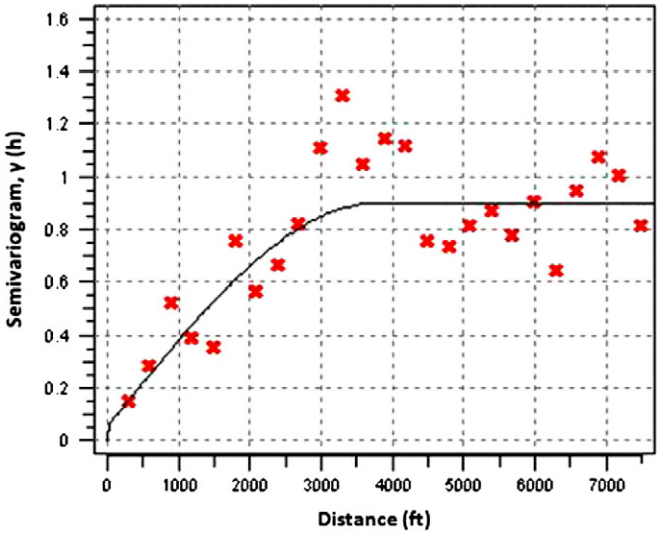

Fig. 14. Experimental semivariogram of surface elevation and the analytical semivariogram representing it. The parameters of the analytical semivariogram are: spherical model, nugget: 0.05, sill contribution: 0.85, maximum range: 3600 ft, medium range: 3420 ft, minimum range: 3330 ft.

Obviously, methane emissions experienced within the active mine cannot originate from gas quantities calculated for the entire area. Therefore, in order to determine in-place gas contents within the boundaries of the mine, active workings were outlined (Fig. 12) in gas-in-place realizations and gas quantities retrieved from 748 grids that belonged to mine area were ranked for quantile estimation. Fig. 13B shows histograms of grid values for Q5, Q50, and Q95 of the outlined mine area. Cumulative gas amounts calculated for these quantiles are 135.1 MMscf, 148.5 MMscf, and 163.7 MMscf, for Q5, Q50, and Q95, respectively. These values can be roughly interpreted as the maximum amount of gas emissions that could be expected from this mine if the entire volume of coal were mined and 100% of the methane was released during mining. However, based on a coal recovery ratio of 40–50% in a room-and-pillar mine, expected emissions should be even less.

Since the start of its operation, the study mine produced approximately 1.021 million tons of coal (MSHA, 2011). Using the estimated specific gas emission of 182.5 scft, the mine generated approximately 186 MMscf of methane. This value is much higher than expected and also higher than total gas-in-place of the mine volume. This suggests that there might be other sources of methane and migration paths for emissions into the active mine.

5.2.2. Sequential Gaussian co-simulation of groundwater level, head, and acidity

It has been shown in Section 3 that this area was affected by tectonic forces and contained folds and faults, which manifested themselves as anticlines and synclines parallel to the Appalachian front. The stresses due to these structures caused fractures in the strata and face cleats in the coal seam(s) to run in the northwest–southeast direction (Figs. 1 and 3). For Lower Kittanning coal, the laboratory permeability values reported in Table 4 were measured along face cleats in this principal direction. In addition, the complexity of the depositional environment resulted in deposition and formation of alternating shales and sandstones, which were separated by transition materials such as slickensides. It has been observed that shale–sand interfaces in the roof of the Lower Kittanning seam contained multiple fissures and fractures due to differential compaction and were also very prone to developing new cracks as a result of any mining-induced stresses.

The characteristics of this area discussed briefly above and offered in detail in previous sections suggest that the sealing capacity of the roof of the Lower Kittanning seam is poor, in that there are multiple fractures providing hydraulic connectivity within and between various strata, and there can be preferential flow directions following cleats and stress-oriented fractures. This suggests that the groundwater can be treated as a single aquifer with preferential flow directions and a saturated zone thickness encompassing various, possibly methane-bearing, formations and coals (such as Kittanning and Freeport coals). These observations are important for evaluating the hydrodynamics of the study area and for predicting how they can impact methane transport and emissions. Similar evaluations were made by Cai et al. (2011) to assess geological controls for predicting coalbed methane accumulation and movement in the Southern Qinshui Basin, China. Their measurements showed that the groundwater movement in the basin is controlled by topography, precipitation, and tectonics. But more importantly, they observed that in recharge and discharge areas, groundwater flow decreased methane content, whereas in deeper parts of the basin, especially in stagnant zones, groundwater trapped methane under pressure. These findings

suggest that coalbed methane can move with groundwater, and thus the hydrodynamics of the area can provide insight into the accumulation and migration of methane.

Two important considerations that impact methane migration from groundwater movement are water level and water head, which describe flow direction and the saturated zone thickness from which methane might be swept at a regional scale, respectively. In this work, water level was monitored at 6 different locations (Obs Wells 1 to 6 in Fig. 5). Monitored water levels at these spatial locations are shown in Fig. 7. Using these data and the elevation of the top of the Lower Kittanning coal at the same locations, water heads can also be calculated. However, six data points for the entire area are too few to predict the direction of water flow and the saturated thickness that can affect methane migration. Therefore, sequential Gaussian simulation and sequential Gaussian co-simulation techniques were used to stochastically model water levels and heads within the entire study area. Acidity was co-simulated, as a surrogate, to assess the impact of abandoned mines in proximity to the active mine on water quality.

For this work, sequential Gaussian co-simulation with the Markov-model-1 (MM1) was selected. MM1 considers the following Markov-type screening hypothesis during simulations: the dependence of the secondary variable on the primary is limited to the co-located primary variable. The cross-covariance is then proportional to the auto-covariance of the primary variable (Remy et al., 2009), which can be shown as:

$$C_{12}(h) = \frac{C_{12}(0)}{C_{11}(0)} C_{11}(h) \tag{3}$$

where h is the distance vector, C_{12} is the cross covariance between the two variables, and C_{11} is the covariance of the primary variable. Thus, solving the cokriging algorithm with MM1 requires the knowledge of correlation between primary and secondary variables, as well as the semivariogram(s) of the primary variable(s). Sequential Gaussian co-simulation allows for simulation of a Gaussian variable, while accounting for the secondary information to which it correlates (Remy et al., 2009). As in Gaussian simulation, Gaussian co-simulation, too, requires Gaussian variables, or calls for them to be transformed to normal scores. Table 9 shows the correlation between normal scores of acidity and water elevation (as primary variables to be co-simulated) and surface elevation (secondary variable). The experimental and analytical semivariograms of surface elevation are given in Fig. 14 and the parameters of the analytical semivariogram are given in its caption.

Important considerations to implement sequential Gaussian co-simulation, with a limited number of primary variables from which correlation coefficients and semivariograms are determined, are discussed at length in Karacan and Olea (in review), who developed a methodology to co-simulate decline curve parameters of gob gas ventholes, and in Olea et al. (2011b), who developed a correlated variables methodology for assessment of gas sources in Woodford shale play, Arkoma basin, in eastern Oklahoma. In the present work, the same methodologies discussed in those papers were applied and thus will not be repeated here in detail. Readers are referred to these papers for detailed discussions.

One hundred realizations were generated for acidity and water level. Water head realizations were generated by subtracting coal top realizations from those of water level elevation. Ranking and

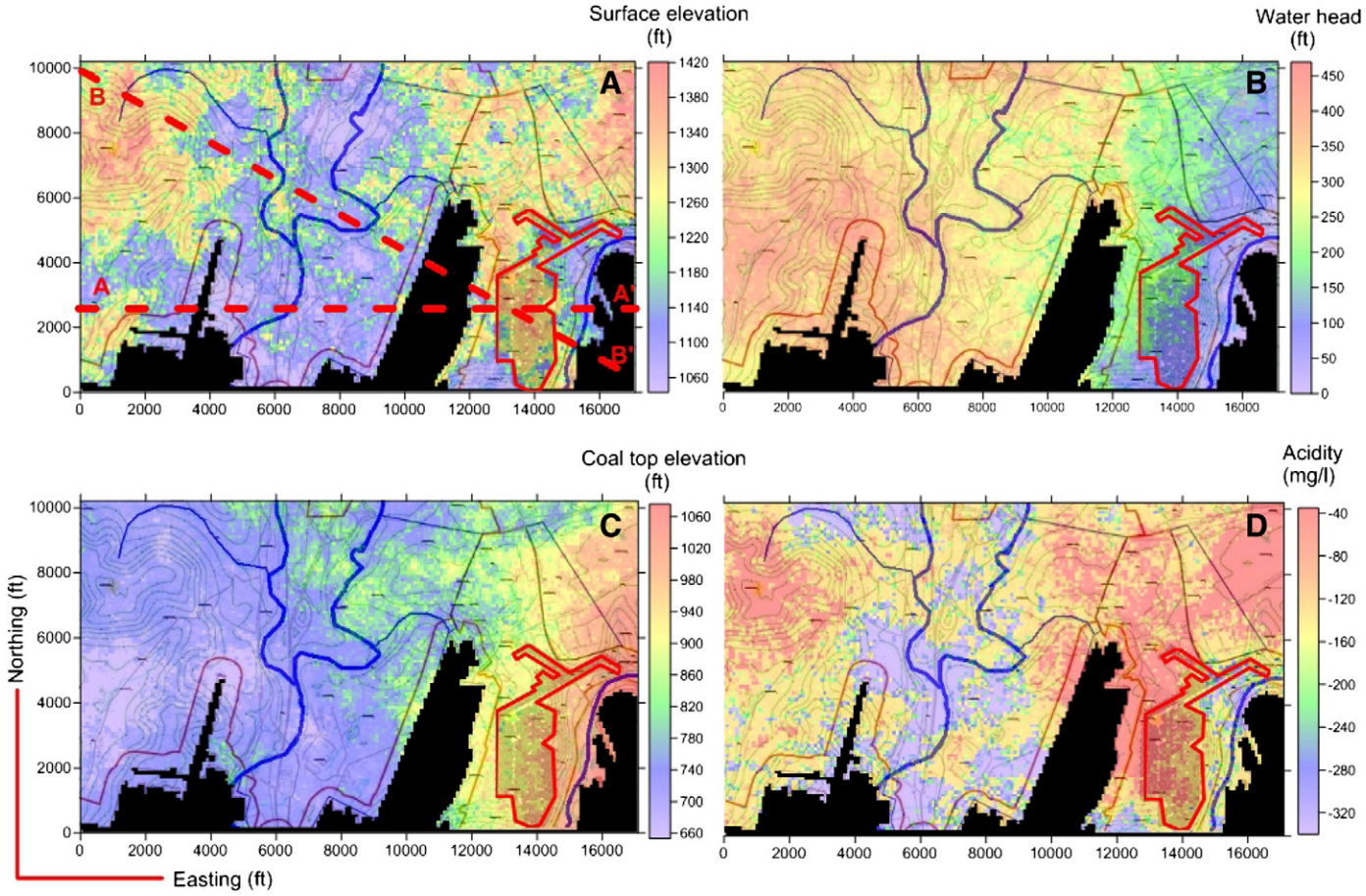

Fig. 15. Q50 realizations of surface elevation, water head, coal top elevation, and acidity. A–A′ and B–B′ profiles shown on the surface elevation map have been used to plot values from various attributes along those directions. Abandoned workings are blanked in black to make their boundaries clear whereas the active mine is outlined in red.

quantile analyses were performed for each of the simulated and co-simulated attributes to determine realizations that correspond to Q5, Q50, and Q95.

Fig. 15 shows Q50 realizations of surface elevation (A), water head (B), coal top elevation (C), and acidity (D). These maps show that surface elevation varies between ~1050 and 1420 ft. The active mine is located under a hilly topography. Elevations in the stream basin and to the east of Yellow Creek are the lowest topographies in the study area. Top of coal elevation (C) shows that the Lower Kittanning seam dips from east to the west in this area with an almost 400-ft difference between the lowest and highest points. The highest location of the coal seam is to the east of the active mine, around Yellow Creek. Water head (or saturated thickness), on the other hand, is highest towards the west of the study area where the difference between simulated water level and top of coal seam is greatest. The height of the water head is around 200 ft on the west margin of the active mine, decreasing to 100–150 ft towards the east entries, and increases to almost 450 ft at the west end of the area (Fig. 15B). These heights indicate that there is a strong water head gradient in the east–west direction and that the thickness of the saturated zone can easily encompass the overlying coal seams, including Upper Freeport coal (Figs. 2 and 4), to mobilize and carry methane along. Fig. 15D shows acidity of the groundwater. This figure indicates that acidity is concentrated more under higher topography, which is not affected by surface streams and flow potentials around them, by comparison to stream basins.

Water level realizations from co-simulations were used to estimate the general direction of groundwater flow which, by definition, is orthogonal to the water level (Valdes et al., 2007) and local hydrodynamics of the area. Spatial autocorrelation analysis for water level was performed and its correlogram was plotted. Spatial autocorrelation analysis reveals the spatial structure of a regionalized variable through a function that quantifies the linear dependence of successive values over spatial locations (Zhang and Selinus, 1998). Autocorrelation of a spatial variable is determined in each direction by increasing the lag distance. The function, correlogram, C (h,s) that defines the variability for all directions is (Valdes et al., 2007):

$$C(h,s) = \frac{1}{N}\sum_{t=1}^{N-h}\left[(x_t - \bar{x})(x_{t+h} - \bar{x})\right] \quad (4)$$

$$C_0(h,s) = \frac{C(h,s)}{\sigma_x^2} \quad (5)$$

$$\sigma_x^2 = \frac{1}{N}\sum_{t=0}^{N}(x_t - \bar{x}) \quad (6)$$

In Eqs. (4)–(6), h is the lag, s is the direction, N is the number of lags in any direction, t is a particular lag count, x is the value at the particular spatial position, $\bar{x}$ is the average of values at a particular angular direction, C_0 (h, s) is the autocorrelation function, and σ_x^2 is the variance of the variable.

Fig. 16 shows Q50 realization of water level (B) and its autocorrelation function (A). The autocorrelation function clearly shows that the regional water level has a structure lying in an approximate direction of 35°N indicated by the dashed arrow. Since flow is, by definition, orthogonal to this direction (Valdes et al., 2007), the general flow direction is ~125°N, as shown with the red arrow in Fig. 16A. It should be noticed that this general flow direction of regional groundwater is towards the southeast through the active mine and also is in the direction of face cleats (Fig. 3) and other oriented structural fractures.

In order to delineate zonal flow patterns, gradients of groundwater level were computed between grids in x and y directions of the model. The data, shown as arrows, were overlaid with the water level map to indicate flow directions (Fig. 16B). This figure shows that there are 3 possible zones of groundwater flow in the general region as indicated by red dashed lines. These zones are east of Stoney Run, the area between Stoney Run and Two Lick Creek, and west of Two Lick Creek. The flow directions are usually oriented towards Two Lick Creek or to Yellow Creek based on gradients as they are the discharge locations in this area.

Due to its importance and proximity to the active mine, the groundwater flow in the east of the study area is more important. The flow directions in Fig. 16B show that the active mine is likely to be in the path of groundwater flow coming in northwest of the mine and also in the path of flow coming from the west, possibly through abandoned workings. Groundwater flowing through the active mine eventually discharges to Yellow Creek on the east of the workings.

In order to demonstrate groundwater flow and interrelations of various attributes, the geostatistical data along the A–A′ and B–B′ profiles shown in Fig. 15A were plotted in Fig. 17. Fig. 17A shows the data along A–A′ profile, whereas Fig. 17B shows the data along B–B′. These profiles were selected based on two general flow directions in the area and also in such a way that they would pass through the active mine to interpret the effects of groundwater on potential methane distribution and migration in the area.

In Fig. 17, the data extracted from multiple attributes were plotted: The top figures show elevations of surface, groundwater, and top of the Lower Kittanning seam. The difference in elevation between groundwater level and the top of the Lower Kittanning coal is the water head, or saturated thickness. The top figures also show the elevation of the top of the Allegheny Group formations (~220 ft above the top of lower Kittanning seam), including all formations and coals shown in Figs. 2 and 4. In these figures, locations of the active mine, abandoned mines, and surface streams were also drawn based on their positions along the profiles, and the direction of water flows deduced from water levels were marked. Fig. 17A and B, middle and bottom plots, show the values of gas-in-place of the

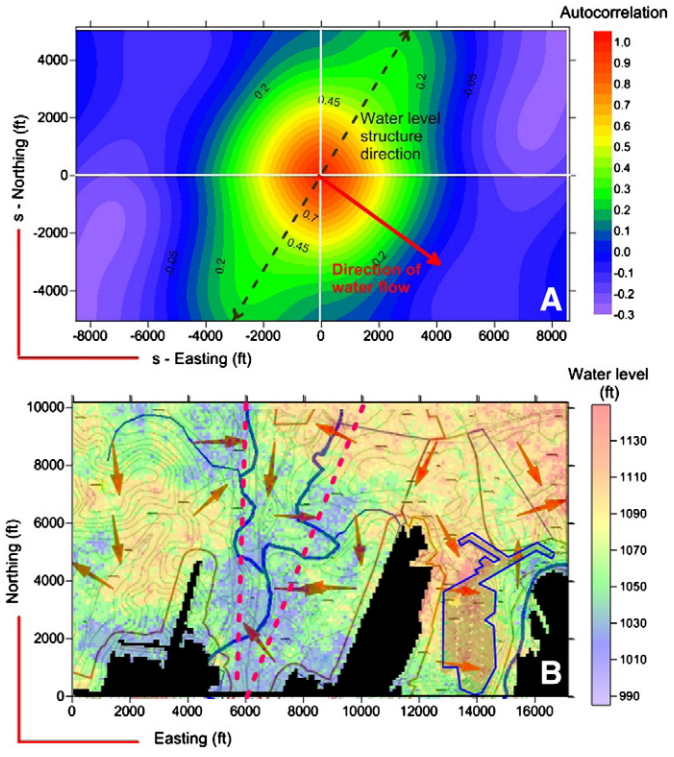

Fig. 16. Autocorrelation of groundwater level and general flow direction (A) and gradients of water level that show zonal flow directions within the study area (B). Again, abandoned mines were blanked and the active mine was outlined.

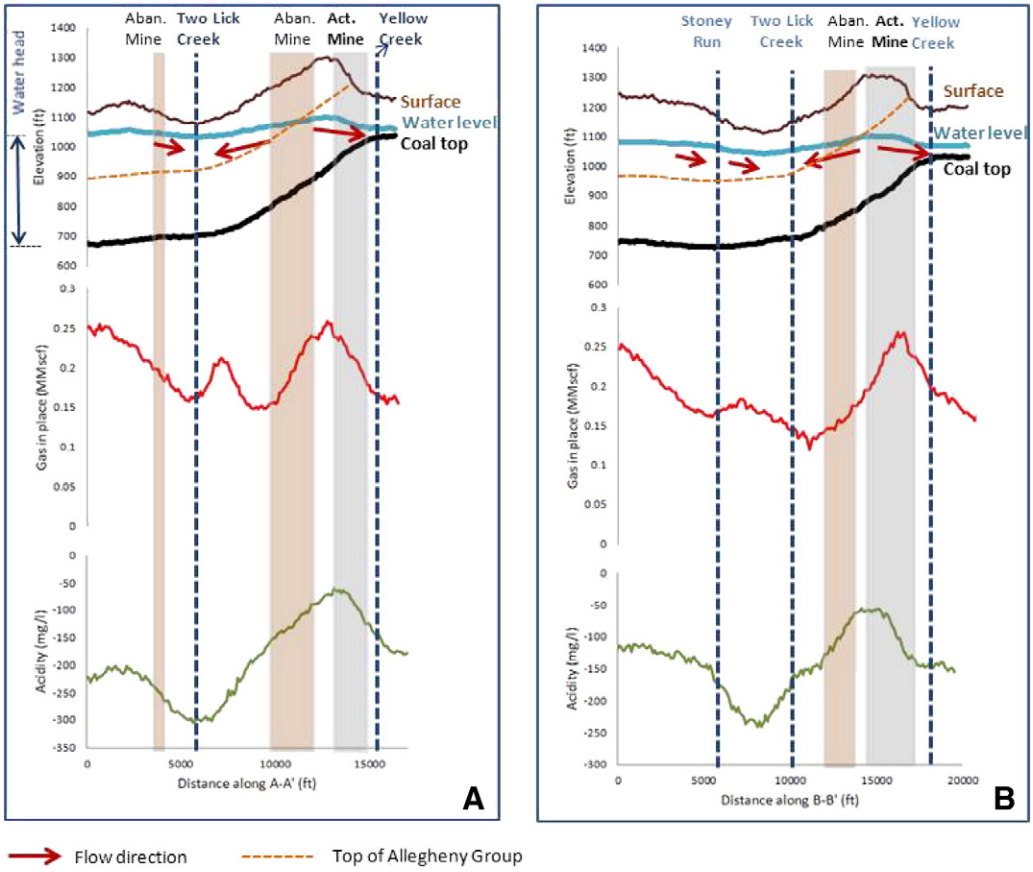

Fig. 17. Elevation and water level data, as well as gas-in-place of the Lower Kittanning seam and acidity of groundwater data extracted from geostatistical simulations along A–A′ and B–B′ profiles shown in Fig. 15.

Lower Kittanning seam and acidity of the groundwater used to interpret them in conjunction with the data given in the top plots.

The data plotted in Fig. 17 show that the groundwater flows towards Yellow Creek and Two Lick Creek as discharge locations in this region. It should also be noticed that the location and elevation of Yellow Creek as a discharge point is so close to the active mine that the groundwater flows through the mine, especially through mine entries in the east, before it meets Yellow Creek. This is important when interpreted with the water head above the Lower Kittanning seam. The data show that the thickness of the saturated zone, or water head, is nearly high enough to cover the entire Allegheny Group formation.

After flowing through the mine workings, groundwater flows towards discharge location. The flow direction shown in Fig. 17 suggests that additional methane observed in the mine might be originated from other coal seams (Middle and Upper Kittanning, and Freeport coals) and carried by the groundwater flow into the workings through cleats, cracks, and fractures within the coals and formations, as well as through openings between shale and sandstones created in the roof during mining. In the western margin of the study area, the groundwater head will be higher and more stagnant flow situations can prevail with regional circulations and discharges to Stoney Run and Two Lick Creek. Thus, methane emissions due to mining in the western part of the study area can more likely reflect the calculated gas-in-place of the Kittanning seam.

These findings and discussions explain the strong role that groundwater may play in the methane emissions experienced in the active mine. They can also explain the effects that water saturation of the cleats, expected to be close to 100% under these circumstances, may have on methane that is liberated only during coal mining despite a ~4 md measured permeability, although it should be treated with caution. These data also suggest that contaminants, such as Fe and SO_4, and water quality parameters, such as acidity, measured in groundwater in observation wells around the active mine might have originated from oxidation of dispersed pyrites of coal-bearing strata of the Allegheny Group, and from abandoned mines within the flow area and subsequently carried by groundwater.

6. Summary and conclusions

A detailed analysis of the methane liberation conditions observed in a Lower Kittanning coal mine was performed. During the course of this study, a geological evaluation of the area was conducted to understand the structural and depositional properties. Coal samples were analyzed for maceral composition, permeability, and gas content. Water samples from 6 water-level monitoring wells were analyzed for geochemical composition and quality parameters. The data from 59 exploration boreholes drilled to the bottom of the Lower Kittanning coal were compiled and evaluated. Statistical and geostatistical modeling were performed to simulate important attributes within the study area.

Structural and depositional characteristics indicated that the area was affected by Appalachian front development and Allegheny orogenesis. These mechanisms resulted in folding and faulting of the study area with the formation of oriented fractures and cleats in the coal seams. In addition, depositional characteristics resulted in formation of shales and sandstones separated by transition materials, i.e. slickensides, which have been observed to cause roof instabilities by developing fractures along the interfaces during mining. The findings indicate that the strata above the coal seams in this area do not have sealing capacity and that these fractures can form an interconnected network for fluid flow.

The gas content of the Lower Kittanning seam changes based on the tested sample. Desorption tests and flotation experiments showed that the top bone coal of the Lower Kittanning coal had high ash and low gas contents (~50 scft). However, the middle and bottom of the seam can contain as much as ~270 scft methane based on depth and rank. Gas-in-place calculated for such areas but excluding bone coal yielded higher gas availability.

Calculated specific gas emission rates, using ventilation methane and coal production data, led to a value of 182 scft of mined coal. This value, when compared with the total gas-in-place of the active mine area, showed that there should be additional methane emissions into the mine resulting in higher than expected specific methane emission rates.

Permeability tests of the Lower Kittanning coal under simulated stress conditions in the laboratory indicated ~4 md permeability. This is normally a high value that should have caused constant methane liberation into the mine from ribs and idle faces. However, methane issuing from active faces only during coal mining suggested that the cleats were saturated with water, thus inhibiting the flow of methane from idle faces.

Temporal water levels monitored at observation wells indicated that there were no seasonal variations in water level, suggesting that recharge and discharge rates were almost similar. This allowed averaged temporal data to be described as only spatial measurements. Water quality data were also treated in a similar manner. This approach used univariate statistics and principal component analyses. Principal component analyses showed that water level and the direction of flow had more influence on the acidic nature of groundwater and Fe and SO_4 quantities. Analyses also suggested that pyrite in overlying coals and coal-bearing formations could be the source of acidity and Fe, both of which are carried by water flow.

Geostatistical simulation and co-simulation with sequential Gaussian techniques were used to model various attributes over the entire study area. These simulations estimated values for gas-in-place and groundwater level. Groundwater level and its correlogram analyses indicated that general flow direction was towards the southeast and the active workings. Modeling the water head indicated that it was high enough to include all Allegheny Group formations within the saturated zone.

Computations of flow gradients showed that the groundwater flows towards Yellow Creek and Two Lick Creek as discharge locations in this region. The location and elevation of Yellow Creek as a discharge point was so close to the active mine that the groundwater flowed through the mine, especially through the east entries, before it met Yellow Creek. This, with the computed water head, indicated that additional methane observed in the mine might have originated from other coal seams (Middle and Upper Kittanning, and Freeport coals) and was carried by groundwater flow into the workings. This finding supports the source and transport of groundwater acidity, Fe, and SO_4.

6.1. Disclaimer

The findings and conclusions in this paper are those of the authors and do not necessarily represent the views of the National Institute for Occupational Safety and Health. Mention of any company name, product, or software does not constitute endorsement by NIOSH.

Appendix A. Supplementary data

Supplementary data associated with this article can be found in the online version, at doi:10.1016/j.coal.2012.04.002. These data include Google maps of the most important areas described in this article.

References

Banks, D., Burke, S.P., Gray, C.G., 1997. Hydrogeochemistry of coal mine drainage and other furriginous water in north Derbyshire and south Yorkshire, UK. The Quarterly Journal of Engineering Geology 30, 257–280.

Bencala, K.E., 2011. Stream–groundwater interactions. In: Widerer, P. (Ed.), Treatise on Water Science, 2. Elsevier, The Netherlands, pp. 537–546.

Berg, T.M., Edmunds, W.E., Geyer, A.R. 1980. Geologic map of Pennsylvania: Pennsylvania Geological Survey, 4th ser., Map 1, scale 1:250,000.

Cai, Y., Liu, D., Yao, Y., Li, J., Qiu, Y., 2011. Geological controls on production of coalbed methane of No. 3 coal seam in Southern Qinshui Basin, North China. International Journal of Coal Geology 88, 101–112.

Carroll, Z.L., Oliver, M.A., 2005. Exploring the spatial relations between soil physical properties and apparent electrical conductivity. Geoderma 128, 354–374.

Code of Federal Regulations, 2009. Mineral Resources. (Title 30§75.325).

Delbari, M., Afrasiab, P., Loiskandl, W., 2009. Using sequential Gaussian simulation to assess the field-scale spatial uncertainty of soil water content. Catena 79, 163–169.

Deutsch, C.V., Journel, A.G., 1998. GSLIB Geostatistical Software Library and User's Guide, 2nd edition. Oxford University Press, New York, NY. (369 pp.).

Diamond, W.P., Levine, J.R., 1981. Direct method determination of the gas content of coal: procedures and results. US Bureau of Mines, Report of Investigations 8515. (36 pp.).

Diamond, W.P., Ulery, J.P., Kravits, S.J., 1992. Determining the source of longwall gob gas: Lower Kittanning Coalbed, Cambria County, Pa. US Bureau of Mines, Report of Investigations 9430. (15 pp.).

Gómez-Hernández, J.J., Cassiraga, E.F., 1994. Theory and practice of sequential simulation. In: Armstrong, M., Dowd, P.A. (Eds.), Geostatistical Simulation. Kluwer Academic Publishers, Dordrecht, pp. 111–124.

Harper, D., Olyphant, G.A., 1993. Statistical evaluation of hydrologic conditions in the vicinity of abandoned underground coal mines around Cannelburg, Indiana. Journal of Hydrology 146, 49–71.

Heriawan, M.N., Koike, L., 2008. Identifying spatial heterogeneity of coal resource quality in a multilayer coal deposit by multivariate geostatistics. International Journal of Coal Geology 73, 307–330.

Hindistan, M.A., Tercan, A.E., Unver, B., 2010. Geostatistical coal quality control in longwall mining. International Journal of Coal Geology 81, 139–150.

Iannacchione, A.T., Ulery, J.P., Hyman, D.M., Chase, F.E., 1981. Geological factors in predicting coal mine roof-rock stability in the Upper Kittanning Coalbed, Somerset County, Pa. US Bureau of Mines, Report of Investigations 8575. (41 pp.).

Karacan, C.Ö., Olea, R.A., Goodman, G.V.R., 2012. Geostatistical modeling of gas emission zone and its in-place gas content for Pittsburgh seam mines using sequential Gaussian simulations. International Journal of Coal Geology 90–91, 50–71.

Karacan, C.Ö., 2008. Modeling and prediction of ventilation methane emissions of U.S. longwall mines using supervised artificial neural networks. International Journal of Coal Geology 73, 371–387.

Karacan, C.Ö., 2009. Degasification system selection for U.S. longwall mines using an expert classification system. Computers and Geosciences 35, 515–526.

Karacan, C.Ö., 2010. Methane control and prediction (MCP) software (version 2.0). http://www.cdc.gov/niosh/mining/products/product180.htm.

Karacan, C.Ö., Olea, R.A. in review. Sequential Gaussian co-simulation of rate decline parameters of longwall gob gas ventholes. International Journal of Rock Mechanics and Mining Sciences.

Kelafant, J.R., Wicks, D.E., Kuuskraa, V.A., 1988. A geological assessment of natural gas from coal seams in the Northern Appalachian coal basin. (Topical report. GRI contract number: 5084-214-1066).

Leuangthong, O., Khan, K.D., Deutsch, C.V., 2008. Solved Problems in Geostatistics. Wiley, Hoboken, New Jersey. (207 pp.).

McCulloch, C.M., Deul, M., 1973. Geologic factors causing roof instability and methane emission problems. The Lower Kittanning Coalbed, Cambria County, Pa. US Bureau of Mines, Report of Investigations 7769. (25 pp.).

Moore, T.D., Deul, M., Kissell, F.N., 1976. Longwall gob degasification with surface ventilation boreholes above the Lower Kittanning Coalbed. US Bureau of Mines, Report of Investigations 8195. (13 pp.).

MSHA, 2011. Mine Data Retrieval System. http://www.msha.gov/drs/drshome.htm.

National Research Council, 2006. Managing Coal Combustion Residues in Mines. The National Academies Press, Washington D.C. (256 pp.).

Olea, R.A., 2006. A six-step practical approach to semivariogram modeling. Stochastic Environmental Research and Risk Assessment 20, 307–318.

Olea, R.A., 2009. A Practical Primer on Geostatistics. U.S. Department of the Interior. U.S. Geological Survey, Open-File Report 2009–1103. (346 pp.).

Olea, R.A., Luppens, J.A., Tewalt, S.J., 2011a. Methodology for quantifying uncertainty in coal assessments with an application to a Texas lignite deposit. International Journal of Coal Geology 85 (1), 78–90.

Olea, R.A., Houseknecht, D.W., Garrity, C.P., Cook, T.A., 2011b. Formulation of a correlated variables methodology for assessment of continuous gas resources with application to the Woodford play, Arkoma Basin, eastern Oklahoma. Boletín Geológico y Minero, Madrid 122 (4), 483–496.

Pennsylvania Geological Survey, 2011. http://www.dcnr.state.pa.us/topogeo/maps/map11.pdf 2011.

Remy, N., Boucher, A., Wu, J., 2009. Applied Geostatistics with SGeMS, A User's Guide. Cambridge University Press, Cambridge, United Kingdom. (264 pp.).

Skema, V.W., Lentz, L.J., Neubaum, J.C., Behr, Rose-Anna, 2008. A study of coal availability in the Clymer 7.5-minute quadrangle, Indiana County, Pennsylvania: Pennsylvania Geological Survey, 4th series, Open-File Report OFMR 08–01.0. (102 pp.).

United States Environmental Protection Agency (EPA), 2004. Methane Emissions from Abandoned Coal Mines in the United States: Emissions Inventory Methodology and 1990–2002 Emissions Estimates. (EPA 430-R-04-001. 54 pp.).

Valdes, D., Dupont, J.P., Laignel, B., Ogier, S., Leboulanger, T., Mahler, B.J., 2007. A spatial analysis of structural controls on Karst groundwater geochemistry at a regional scale. Journal of Hydrology 340, 244–255.

Wackernagel, H., 2010. Multivariate Geostatistics — An Introduction with Applications, 3rd edition. Springer, Berlin, Germany. (387 pp.).
Webster, R., Oliver, M.A., 2007. Geostatistics for Environmental Scientists, 2nd edition. Wiley, West Sussex, England. (330 pp.).
Worrall, F., Pearson, D.G., 2001. The development of acidic groundwaters in coal-bearing strata: Part 1. Rare earth element fingerprinting. Applied Geochemistry 16, 1465–1480.
Younger, P., 2000. Predicting temporal changes in total iron concentrations in groundwaters flowing from abandoned deep mines: a first approximation. Journal of Contaminant Hydrology 44, 47–69.
Zhang, C., Selinus, O., 1998. Statistics and GIS in environmental geochemistry — some problems and solutions. Journal of Geochemical Exploration 64, 339–354.